A 2D Ultrasound Transducer with Front-End ASIC and Low Cable Count for 3D Forward-Looking Intravascular Imaging

Performance and Characterization

Janjic, Jovana; Tan, Mingliang; Daeichin, Verya; Noothout, Emile; Chen, Chao; Chen, Zhao; Chang, Zu-yao; Beurskens, Robert H.S.H.; van Soest, Gijs; van der Steen, Antonius F.W.

DOI
10.1109/TUFFC.2018.2859824

Publication date
2018

Document Version
Final published version

Published in
IEEE Transactions on Ultrasonics, Ferroelectrics, and Frequency Control

A 2-D Ultrasound Transducer With Front-End ASIC and Low Cable Count for 3-D Forward-Looking Intravascular Imaging: Performance and Characterization

Jovana Janjic, Mingliang Tan, Verya Daeichin, Emile Noothout, Chao Chen, Zhao Chen, Zu-Yao Chang, Robert H. S. H. Beurskens, Gijs van Soest, Antonius F. W. van der Steen, *Fellow, IEEE*, Martin D. Verweij, *Member, IEEE*, Michiel A. P. Pertijs, *Senior Member, IEEE,* and Nico de Jong, *Member, IEEE*

***Abstract*— Intravascular ultrasound (IVUS) is an imaging modality used to visualize atherosclerosis from within the inner lumen of human arteries. Complex lesions like chronic total occlusions require forward-looking IVUS (FL-IVUS), instead of the conventional side-looking geometry. Volumetric imaging can be achieved with 2-D array transducers, which present major challenges in reducing cable count and device integration. In this work, we present an 80-element lead zirconium titanate matrix ultrasound transducer for FL-IVUS imaging with a front-end application-specific integrated circuit (ASIC) requiring only four cables. After investigating optimal transducer designs, we fabricated the matrix transducer consisting of 16 transmit (TX) and 64 receive (RX) elements arranged on top of an ASIC having an outer diameter of 1.5 mm and a central hole of 0.5 mm for a guidewire. We modeled the transducer using finite-element analysis and compared the simulation results to the values obtained through acoustic measurements. The TX elements showed uniform behavior with a center frequency of 14 MHz, a −3-dB bandwidth of 44%, and a transmit sensitivity of 0.4 kPa/V at 6 mm. The RX elements showed center frequency and bandwidth similar to the TX elements, with an estimated receive sensitivity of 3.7 μV/Pa. We successfully acquired a 3-D FL image of three spherical reflectors in water using delay-and-sum beamforming and the coherence factor method. Full synthetic-aperture acquisition can be achieved with frame rates on the order of 100 Hz. The acoustic characterization and the initial imaging results show the potential of the proposed transducer to achieve 3-D FL-IVUS imaging.**

***Index Terms*— Forward looking (FL), front-end application-specific integrated circuit (ASIC), intravascular ultrasound (IVUS), piezoelectrical transducer.**

Manuscript received April 25, 2018; accepted July 12, 2018. Date of publication July 25, 2018; date of current version October 3, 2018. This work was supported in part by the Dutch Technology Foundation STW under Grant 12710, which is part of the Netherlands Organization for Scientific Research (NWO), and in part by the Ministry of Economic Affairs. *(Corresponding author: Jovana Janjic.)*

J. Janjic, R. H. S. H. Beurskens, G. van Soest, and A. F. W. van der Steen are with the Thoraxcenter, Department of Biomedical Engineering, Erasmus University Medical Center, 3015 CN Rotterdam, The Netherlands (e-mail: j.janjic@erasmusmc.nl; r.beurskens@erasmusmc.nl; g.vansoest@erasmusmc.nl; a.vandersteen@erasmusmc.nl).

M. Tan, C. Chen, Z. Chen, Z.-Y. Chang, and M. A. P. Pertijs are with the Electronic Instrumentation Laboratory, Delft University of Technology, 2628 CD Delft, The Netherlands (e-mail: mingliangtan0215@gmail.com; c.chen-3@tudelft.nl; z.chen-3@tudelft.nl; z.y.chang@tudelft.nl; m.a.p.pertijs@tudelft.nl).

V. Daeichin and E. Noothout are with the Laboratory of Acoustical Wavefield Imaging, Delft University of Technology, 2628 CJ Delft, The Netherlands (e-mail: e.c.noothout@tudelft.nl).

M. D. Verweij and N. de Jong are with the Laboratory of Acoustical Wavefield Imaging, Department of Imaging Physics, Delft University of Technology, 2628 CJ Delft, The Netherlands, and also with the Thoraxcenter, Department of Biomedical Engineering, Erasmus University Medical Center, 3015 CN Rotterdam, The Netherlands (e-mail: m.d.verweij@tudelft.nl; n.dejong@erasmusmc.nl).

Digital Object Identifier 10.1109/TUFFC.2018.2859824

I. Introduction

ISCHEMIC heart disease is the leading cause of morbidity and mortality worldwide [1], caused by reduced blood flow in the coronary arteries that supply the heart. The development of atherosclerotic plaques within the coronary arteries leads to either a gradual narrowing of the free lumen or sudden blockage due to plaque rupture and subsequent thrombosis [2], [3]. Intravascular ultrasound (IVUS) is nowadays employed to assess the pathophysiology of atherosclerosis from within the vessel lumen, and to guide minimally invasive therapeutic interventions with stents [4]. IVUS is an imaging modality that uses a small catheter (approximately 1 mm diameter) with an integrated ultrasound transducer to visualize arteries from inside. Most commercially available IVUS catheters provide a cross-sectional view of the vessel. This is achieved by rotating a single-element transducer, mounted on the side of the catheter and transmitting ultrasound waves in the radial direction from the catheter. The ultrasound waves are then reflected back from the vessel wall to the transducer [5], [6]. An electronically steered IVUS catheter also exists (Eagle Eye, Volcano Therapeutics) consisting of an array of 64 transducer elements mounted around the tip of the catheter and interfaced with integrated circuits requiring seven electrical wires [7], [8].

Side-looking IVUS catheters are restricted to use in nonocclusive lesions by their imaging geometry, limiting their application in the treatment of very complex lesions, such as chronic total occlusions (CTOs) [9]. CTOs are plaques that have grown to completely fill the vessel lumen. They typically have a highly heterogeneous tissue composition, with variable

mechanical properties and presence of microchannels [10]. Treatment consists of passing the lesion with a thin (0.3 mm) guidewire and opening the vessel with a balloon and stent. Imaging the plaque with forward-looking (FL) ultrasound transducers, integrated into a steerable catheter may direct the physician to optimal locations for wire entry, providing imaging guidance during the crossing procedure and enhancing the device dexterity.

Early work in the development of FL-IVUS consisted of single-element transducers with a rotating mechanism that is either converted into a scanning motion of the FL element [11], [12] or directly applied to rotate an element oriented at a 45° angle [13]. In the first case, 2-D FL scans can be achieved, whereas with the second approach a cone of visualization is created ahead of the catheter tip. Other approaches for single-element FL imaging include a rotating reflecting surface [14] that reflect the ultrasound beam with different angles ahead of the catheter tip and a mechanically wobbling transducer with shape-memory alloys [15]. These approaches require the need to develop complex mechanisms, making the whole catheter bulky.

Considerable effort has been put into the development of multielement arrays, which do not need rotation. Miniaturized linear arrays that provide 2-D FL ultrasound images [16]–[18] can achieve volumetric imaging by mechanically scanning the transducer and combining different 2-D planes into a 3-D volume data set. This procedure is complex and easily affected by motion artifacts. The 2-D matrix transducers can provide volumetric imaging without moving the probe. However, integration of multielement transducers in intravascular catheters is challenging because of the complexity of wiring the many elements to a signal acquisition system. Matrix and ring arrays with approximately 100 individually connected elements have been pioneered for IVUS applications [19], [20]. However, there is usually not enough space in the catheter for these large wire assemblies. Electronic circuits with pulsers and multiplexers, integrated with the 2-D matrix transducer, can reduce the cable count. This approach has been used in the development of FL intravascular and intracardiac transducers based on capacitive micromachined ultrasonic transducers (CMUT) [21]–[27], which are fabricated using silicon-based technologies and can be cointegrated with front-end electronics to reduce the interconnection complexity [28], [29]. FL CMUT-based transducers for intravascular and intracardiac applications requiring 13 wires have been proposed [25], [26].

In an elegant combination of a side-looking and a FL array [30], [31], the distal part of a 64-element circular side-looking array was cut and used to generate forward waves in the 3-1 mode. With the resulting annular array, the number of transceiver firings can be optimized to yield 3-D FL imaging with reasonable side and grating lobe level (−20-dB sidelobe and almost −30-dB grating lobe level at a steering angle of 30°). Experimentally, a sidelobe level of approximately −15 dB was realized, probably due to missing elements [31]. Moreover, since 3-D FL imaging is achieved using only a narrow ring of elements, power dissipation and sensitivity remain a concern.

An intracardiac side-looking lead zirconium titanate (PZT)-based array with an application-specific integrated circuit (ASIC) has been integrated into a 10 Fr (3.3 mm) steerable catheter and tested *in vivo* [32]. This device consists of a 2-D matrix transducer with an aperture of 2.5×6.6 mm^2, a pitch of 180 μm, and a center frequency of 5.6 MHz. The element-matched connection with the ASIC was realized via a flexprint and a dematching layer between the ASIC and the PZT in order to minimize the acoustic energy transport into the backing.

Next to FL imaging, minimally invasive procedures could benefit from steerability of intravascular devices. Single-element FL imaging using a steerable catheter and an optical shape-sensing system has been demonstrated in a previous publication by our group [33]. For each degree of freedom (DOF), two pulling wires are required. To accommodate multiple pulling wires, hence improving device dexterity, it is important to reduce the number of coaxial cables.

We propose here a PZT-based FL-IVUS matrix transducer built on a front-end ASIC that requires only four micro-coaxial cables to address a 2-D matrix array with a total of 80 elements. The micro-coaxial cables could easily fit in an intravascular catheter and leave space for a guidewire and up to eight pulling wires, hence enabling steering with four DOFs. The PZT has been mounted directly on the ASIC with gold ball contacts and conducting glue resulting in a shorter rigid segment at the tip compared to [7] and [8]. The ASIC and transducer have been designed in conjunction, as their mutual performance is tightly linked. The electronic design of the ASIC was reported previously [34]. In this paper, we focus on the design, the fabrication process, and the quantitative characterization of the FL-IVUS transducer built on top of the ASIC. We also performed FL volumetric imaging of three spherical reflectors in water.

In Section II, we investigate different transducer designs using field-II simulations [35]–[37]. Based on the simulation results, we estimate the effects of a practical implementation and we present the final device design, the finite-element analysis (FEA) model used to simulate the acoustic behavior, and the experimental setup for ultrasonic characterization in Section III. FEA and measurement results are presented in Section IV, and the discussion and conclusions are given in Section V.

II. Optimal Transducer Layout Analysis

Intracoronary ultrasound catheters have a maximum outer diameter of 1.5 mm and should accommodate a ∼0.3–mm-diameter flexible guidewire for accurate delivery. To meet these requirements, the most suitable approach is to build the transducer directly on top of an ASIC, similar to [23] and [25]. The envisioned block diagram of the ASIC is shown in Fig. 1.

The ASIC will employ HV switches to connect one or multiple transmit (TX) elements to an external pulser, whereas a multiplexer will connect one of the receive (RX) elements to an analog front-end (AFE) that consists of a transimpedance amplifier (TIA) with very small input impedance, a programmable gain amplifier (PGA) with three gain settings, and a

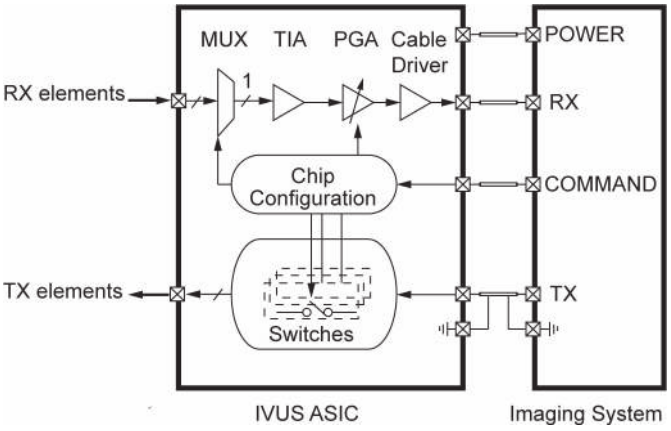

Fig. 1. Block diagram of the ASIC. MUX: multiplexer, TIA: transimpedance amplifier, and PGA: programmable gain amplifier. The ASIC requires only four cables to connect the 2-D matrix transducer to the external imaging system.

TABLE I
FL-IVUS TRANSDUCER REQUIREMENTS AND CONSTRAINTS

Requirements		Constraints	
center frequency	14 MHz		
pitch	< λ	min. pitch	100 μm
outer diameter	1.5 mm	max. num. of TX	16
inner hole diameter	0.5 mm	max. num. of RX	100

buffer which serves as a cable driver. The ASIC should enable synthetic-aperture imaging where acoustic pulses are transmitted using one or multiple TX elements, and the reflected echoes are received by the RX elements one element at a time. Beside the described analog approach, the ASIC will also be capable of locally digitizing the received signals, providing more robust signal transmission [34]. However, since the main focus of this work is the acoustic characterization of the 2-D matrix transducer on top of the ASIC, we considered the ASIC in analog mode only.

Considering the available area for the ASIC and the dimensions of each chip components, we estimated that the ASIC could address a maximum of approximately 100 receive elements. This number can only be achieved by minimizing the number of transmit elements since the high-voltage (HV) switches are the largest components (approximately 100 × 100 μm^2) occupying the ASIC area. Based on these considerations, the maximum number of transmit elements was set to 16.

The target center frequency is 14 MHz, which is lower than standard IVUS frequencies (20–40 MHz), but can provide more penetration depth suitable for FL imaging [26], [30]. For reduced grating lobes, a pitch smaller than the wavelength λ is desirable. However, the available transducer fabrication process, which is described later, limits the pitch to a minimum of 100 μm. We summarize the transducer requirements and the constraints due to the ASIC and the fabrication process in Table I.

TABLE II
INVESTIGATED TRANSDUCER DESIGNS

Design Type	Layout (TX in yellow, RX in red)	TX elements	RX elements
A	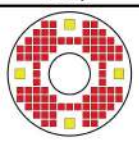	4 (100 X 100 μm)	84 (80 X 80 μm)
B		12 (80 X 80 μm)	88 (80 X 80 μm)
C	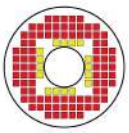	16 (80 X 80 μm)	88 (80 X 80 μm)
D	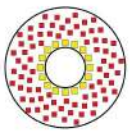	16 (60 X 60 μm)	77 (60 X 60 μm)

With these considerations in mind, we investigated, through ultrasound field simulations in field-II, different 2-D matrix designs. The investigated designs are described in Table II. In the first three designs, the TX and the RX elements were arranged on a regular grid with a pitch of 100 μm and a kerf of 20 μm. Transducers with these layouts can be manufactured using a diamond dicing saw. The last design consisted of TX and RX elements arranged in a nongridded pattern. In particular, the receivers were placed according to a tapered spiral pattern [38] with variable pitch ($\geq$100 μm). A transducer with this configuration can be manufactured with laser cutting technology.

For each design, we computed the pulse-echo (PE) beam profile on a half spherical surface with a radius of 6 mm [Fig. 2(a)] and we simulated the 3-D synthetic-aperture imaging of three point scatterers [Fig. 2(b)]. The transducer is simulated in the xy plane with z the propagation axis. For each PE beam profile, we also extracted the maximum sidelobe level at each elevation angle as shown in Fig. 3.

In design ***A***, where four TX elements are organized at the top, bottom, left, and right side of the transducer aperture, the simulated PE field showed maximum sidelobe levels of −15 dB at approximately 10° as shown in Fig. 3. Increasing the number of TX elements and positioning them in a cross-like pattern (design ***B***) reduced the maximum sidelobe level to approximately −19 dB. However, the beam profile showed still a significant spread in the energy around the main beam as shown in Fig. 2. By positioning the TX elements around the inner hole (designs ***C*** and ***D***), both the sidelobe level and the beam spread were reduced. The nongridded configuration of the RX elements in design ***D*** gave the narrowest beam spread

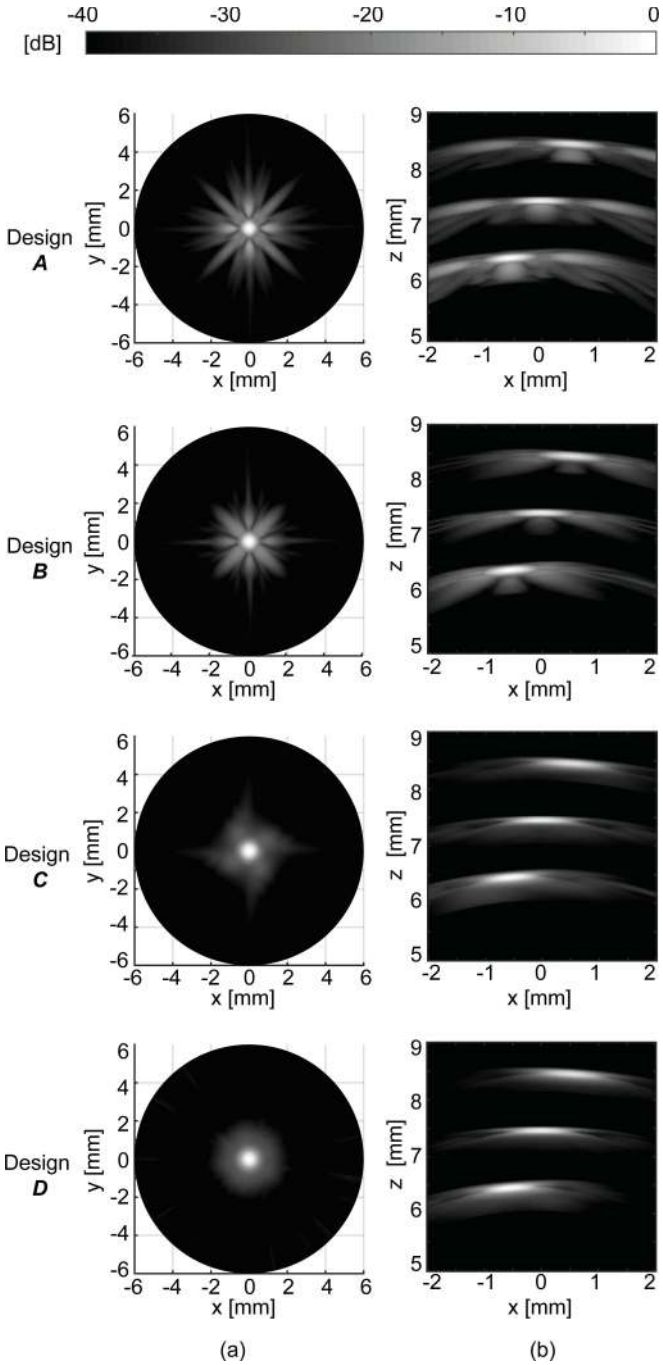

Fig. 2. (a) Simulated PE profiles on a half spherical surface with a radius 6 mm. (b) Maximum projections along y-axis of simulated synthetic-aperture images of three point scatterers.

and the smallest sidelobe level. Nevertheless, the improvement over design ***C*** was not as significant as compared to the other designs. Laser cutting transducer elements which are mounted on top of an ASIC are not trivial and require accurate control of the cutting depth to avoid damage to the chip. On the other side, the cutting depth of the mechanical dicing saw can be more easily controlled.

Therefore, in this work, we opted for design ***C*** to prove the concept of 3-D FL-IVUS imaging using a 2-D matrix transducer with a front-end ASIC and a low cable count.

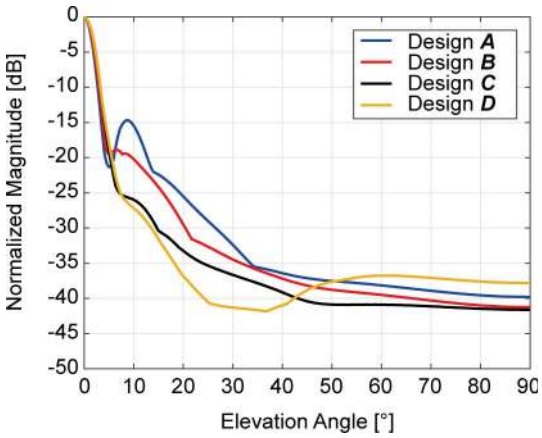

Fig. 3. Maximum lobe level at each elevation angle. Curves are extracted from Fig. 2(a).

TABLE III
COMPARISON WITH PRIOR WORK

	Design C	[30] and [31]	[19]	[25]
Frequency [MHz]	14	10	10	20
Diameter [mm]	1.5	1.3	1.6	1.4
Number of cables	4 (coaxial)*	7	97 (coaxial)	13
Number of elements	82	64	97	104
Vibrating mode / relative sensitivity	d_{33} / 100%	d_{31} / 50%	d_{33} / 100%	-
Proposed number of firing	1024	210	-	672
Grating lobe level at 30 deg steering [dB]	-30	-30	-	<-40
Construction	PZT on ASIC	PZT on flexprint	PZT on flexprint	CMUT on ASIC

*Although measurements were done with 4 coax cables, the chip can operate with 3 coax cables and 1 unshielded power cable

A comparison of our approach with previous work is provided in Table III. Our proposed transducer with front-end ASIC requires the lowest number of cables and, using the highest number of firings (1024), results in grating lobes of approximately −30 dB when steering by 30° with frame rates suitable for real-time imaging (∼100 Hz).

III. TRANSDUCER DESIGN AND CHARACTERIZATION

A. Final Transducer Layout

The final transducer design was further adjusted to accommodate the five bond pads for the ASIC connection to four micro-coaxial cables and to ground. Since these pads, in the current ASIC design, are located on the same side of the

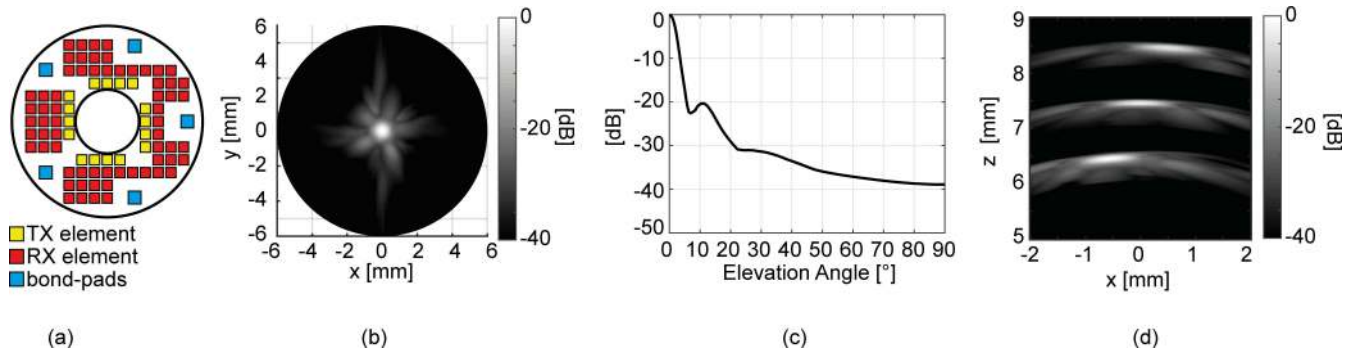

Fig. 4. (a) Final design layout. (b) Simulated PE beam profile over a half spherical surface with radius 6 mm. (c) Extracted maximum sidelobe level for each angle. (d) Maximum projection of a simulated full synthetic-aperture image of three point scatterers.

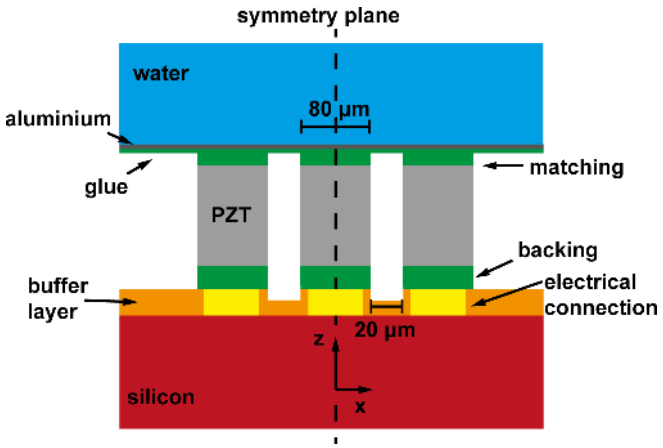

Fig. 5. 3-D FEA model in the *xz* plane.

ASIC as the transducer array, transducer elements could not be placed at their location. Each pad has a size of 100 μm $\times$ 100 μm and a safety distance of 70 μm from the transducer elements.

To integrate the five bond pads in the limited chip area, the number of RX elements was decreased to 64, leading to a design that had a total of 80 elements (16 TX and 64 RX elements) with an element size of 80 μm $\times$ 80 μm and a pitch of 100 μm $\times$ 100 μm. The layout is shown in Fig. 4 together with the simulated PE beam profile and the maximum projection from a synthetic-aperture image of three scatterers. The -6-dB lateral width of the point scatterer at 6.5 mm is 540 μm.

The changes in the layout due to the inclusion of the bond pads lead to a spread in energy around the main beam and an increase in the sidelobe level compared to design ***C*** (Fig. 2). However, the maximum sidelobe level at 10° is below -20 dB [Fig. 4(c)], which is still better than both designs ***A*** and ***B***.

B. Finite-Element Modeling

We modeled the transducer on top of the ASIC and simulated its acoustic performance using FEA software (PZFlex LLC, Cupertino, CA, USA). The 3-D model geometry consisted of three transducer elements where only the central one is active (Fig. 5). The layer stack consists of, bottom to top, the silicon substrate containing the ASIC, a nonconductive epoxy filling the gaps between the electrical connections, a conductive adhesive backing, the PZT active layer, a conductive matching layer, and a thin aluminum ground electrode. The kerfs between the elements were kept void, and the overall transducer was loaded with water. The material properties and thicknesses of each layer are described in Table IV.

TABLE IV
THICKNESSES AND MATERIAL PROPERTIES USED IN THE FEA SIMULATIONS

Material	Thickness	Properties
Silicon	300 µm	ρ=2330 kg/m^3, c_p=7526 m/s, c_s=4346 m/s
Gold (Electrical connection)	30 µm	ρ=19700 kg/m^3, c_p=3240 m/s, c_s=1200 m/s
Buffer epoxy	30 µm	ρ=2220 kg/m^3, c_p=2613 m/s, c_s=1289 m/s
Conductive glue	Backing: 40 µm Matching: 20 µm Top of Matching: 7 µm	ρ=3330 kg/m^3, c_p=1873 m/s, c_s=970 m/s
PZT CTS3203HD	100 µm	ρ=7820 kg/m^3 c_{11}=137, c_{12}=88, c_{13}=92, c_{33}=126, c_{44}=22, c_{66}=25 MPa ε_{11}=1306, ε_{33}=1200 C/Vm e_{15}=16, e_{31}= 9, e_{33}=22 C/m^2
Aluminium (ground connection)	7 µm	ρ=2690 kg/m^3, c_p=6306 m/s, c_s=3114 m/s

The mesh used in PZFlex has a spatial resolution of 2 μm that was achieved by considering 15 grid elements per minimum wavelength for the lowest occurring speed of sound of 1482 m/s and a maximum frequency of 50 MHz. To reduce the simulation time, we assumed symmetry in the planes $x = 0$

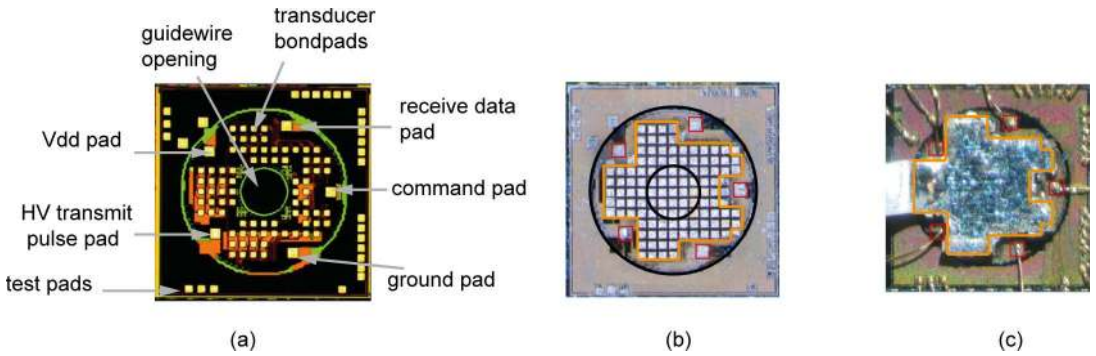

Fig. 6. (a) ASIC micrograph. (b) Matrix array on top of the ASIC after dicing. (c) Matrix array after ground foil application and wire bonding. Bond pads for the cables are highlighted in red, whereas the transducer aperture is delimited by orange lines.

and $y = 0$; hence, only a quarter of the model needed to be simulated.

To study the transmit performance of the single-element, a half-period sinusoidal pulse with a 28-V_{pp} amplitude and a pulsewidth of 25 ns is applied to the element. The -3-dB fractional bandwidth of the pulse is approximately 180%. Using the Kirchhoff extrapolation technique [39], the simulated pressure at the surface is propagated into water over 6 mm in the axial direction. Using PZFlex, we also extrapolated the element impedance at resonance, which was used to design the AFE in the ASIC.

The receive behavior of the individual element is investigated through simulations by defining close to the transducer surface the same pressure load that was obtained from the measurements in transmission. For these simulations, we also took into account the input impedance of the AFE in the ASIC. First, a SPICE-type simulator (Spectre Circuit simulator, Cadence Design Systems, Inc., San Jose, CA 95134, USA) was used to obtain the magnitude and phase of the AFE input impedance over different frequencies. Then, we fit the resulting value to an *RC* equivalent circuit, which was modeled in PZFlex as connected in parallel to the element.

C. Transducer Fabrication

The fabrication process of the 2-D matrix on top of the ASIC was based on the PZT-on-CMOS integration described in [40]. Briefly, the bond pads on the ASIC that are used to electrically connect each individual element were arranged in the same configuration and with the same pitch as the transducer matrix layout [Fig. 6(a)].

Metal studs were applied on top of the bond pads and the gap in between was then filled with nonconductive epoxy (5.8 MRayl, Oldelft B.V., Delft, The Netherlands). The excess epoxy was grinded down to expose the metal and form electrical contacts. A next layer of conductive glue (6.2 MRayl, Oldelft B.V., Delft, The Netherlands) was used to electrically connect the back electrode of the PZT to the electrical connections on the ASIC. This procedure is very delicate since the conductive glue should not cover the five bond pads [red squares in Fig. 6(b)] that will be wire bonded later on for electrical connection.

The individual elements PZT (CTS3203HD) elements were cut with a dicing saw until the buffer layer and the kerfs were left void. The entire matrix was then covered with a ground foil to create a common ground electrode for all the elements. Due to the fabrication process, diced transducer elements without electrical connection were also present in the inner hole reserved for the guidewire [Fig. 6(b)]. An extra step should be considered in the future to remove these elements when integrating the transducer in a catheter with a guidewire, ideally employing laser cutting techniques to minimize the damage to those elements located at the edge of the inner hole. The chip with the transducer was then mounted on a custom printed circuit board (PCB) for testing purposes, and from the five bond pads on the ASIC, 18-μm-thick aluminum wire bonds were used to provide electrical connection to the PCB [Fig. 6(c)].

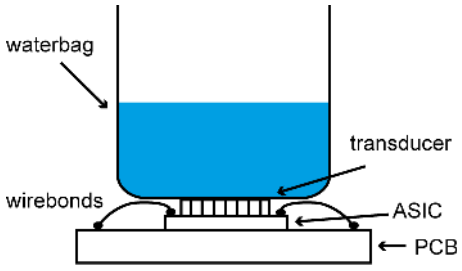

Fig. 7. Measurement setup.

D. Measurement Setup

The measurement setup is depicted in Fig. 7. A small water bag made of acoustically transparent material was placed on top of the 2-D FL-IVUS transducer, which was mounted on the PCB.

To characterize the TX elements in terms of transmit sensitivity, bandwidth, center frequency, and directivity, a 75-μm needle hydrophone (SN1302, Precision Acoustics, Dorchester, U.K.) was placed in the water bag above the transducer using a positioning stage (Newport Corporation, Irvine, CA, USA) that allowed placing the hydrophone accurately 6 mm away from the transducer surface. Each transducer element was excited with a pulser (AVIR-4D-B, Avtech Electrosystems Ltd, Ogdensburg, New York, USA) that was manually programmed to generate a unipolar pulse with a width of 25 ns and an amplitude of 28 V, as measured on the PCB.

The external transmit pulse was then delivered to the specific transmit element through the HV switches on the ASIC. The acoustic pressure recorded by the hydrophone was amplified by a 58-dB amplifier (AU1519, Miteq, Long Island, New York, USA), recorded by a digital oscilloscope (DL9710L, Yokogawa, Tokyo, Japan) and transferred to a PC. To acoustically characterize the center frequency and bandwidth of the RX elements, the hydrophone was replaced by a tungsten wire (50 μm) that was mounted parallel to the surface of the transducer. PE measurements were performed with all the TX elements excited simultaneously, whereas the signals received from each RX element were recorded one by one. The transmit pulse was the same as in the hydrophone measurement except that the switches on the ASIC connected the external pulse to all the transmit elements simultaneously. The echo reflected back from the wire was converted by each element into an electrical signal that was transferred via a multiplexer to the AFE. The received signal was amplified by 18 dB through the PGA and stored on the PC. For both the TX and RX measurements, the signal stored on the PC was digitally filtered with a 5–30-MHz passband filter. To identify the functional elements, for each A-line, we computed the signal-to-noise ratio (SNR) as the ratio of the rms amplitude value in a region including the transducer element signal over the rms amplitude in a region without the element signal. The elements with an SNR more than 6 dB below the mean value were identified as not working; hence, they were not considered further in the analysis.

To measure the receive sensitivity, a flat steel plate was placed in the water bag on top of the transducer and PE measurements were performed transmitting with a single TX element and receiving with the neighboring RX element. The output signal V_{out} of the receive element can be expressed as

$$V_{\text{out}} = P_{\text{in}} S_{\text{rx}} G$$

where P_{in} is the acoustic pressure at the element, S_{rx} is the element receive sensitivity, and G is the electric circuit gain. To decouple the performance of the RX element from the performance of the receive electronics on the ASIC, we first computed the transfer function of the AFE using the response measured on one of the test inputs available on the ASIC [Fig. 6(a)], while keeping the RX elements disconnected from the AFE. Using an arbitrary waveform generator (33522A, Agilent, Santa Rosa, CA, US) and a manual step attenuator (355D, Agilent, Santa Rosa, CA, US) set to 20 dB, we applied to the test input 3-cycle sinusoidal burst signals with a frequency varying from 10 to 20 MHz and with four different peak-to-peak amplitudes (50, 100, 200, and 500 mV). Since the LNA chosen for the ASIC was a TIA, an on-chip resistor was implemented to convert the external test voltage signal into a current. Both the input and output voltages were recorded through the oscilloscope. The ratio between their amplitudes was used to compute the analog gain at different frequencies, obtaining the transfer function of the electric circuit chain. Based on that, we divided the PE signal recorded from the flat steel reflector by the AFE gain, yielding the current signal out of each transducer element. The measured current was then compared to the theoretical result computed through PZFlex simulations.

We also measured the input referred noise spectrum of the analog receive chain, and we compared it to the simulated value from the SPICE-type simulator. In addition, by sweeping the test input signal from 1 nA to 6 μA, we computed the dynamic range under the three gain settings of the PGA available.

To test the imaging capabilities of the matrix transducer, three needles with steel spheres at the tip were placed in the water bag at different distances from the transducer surface and 3-D FL imaging was performed with only four cables interfacing the 16 TX elements and the 64 RX elements. The synthetic-aperture imaging scheme was as follows: each of the 16 TX elements was excited individually and the echoes received by the 64 RX elements were acquired in 64 successive PE sequences. The resulting RF lines were beamformed resulting in a low-resolution volume for each transmit element. The final volume was obtained by averaging the 16 low-resolution volumes.

Images were created by beamforming the received echoes by the traditional delay-and-sum (DAS) approach and by coherence factor (CF) weighting [41] applied to the delayed lines before summation. We then compared the measured -6-dB lateral width to the values obtained from field-II simulations.

IV. Transducer Performance Evaluation

A. Transmit Characterization

The simulated transmit acoustic pressure wave obtained in PZFlex is shown in Fig. 8(a), whereas Fig. 8(b) shows the pressure wave measured with the hydrophone for a representative TX element. The measured SNR [Fig. 9(a)] together with the center frequency and -3-dB bandwidth of each TX element [Fig. 9(b)] demonstrates the functionality and the low variation across the 16 TX elements. Fig. 9(c) shows the measured directivity of five transmit elements together with the averaged directivity pattern. The -6-dB angle was measured to be approximately $\pm 30°$.

Table V compares the average values from the measurements to the simulated values in terms of center frequency, bandwidth, and peak-to-peak pressure at 6 mm, showing good agreement between the values. Based on the measured pressure and the input voltage amplitude, we estimate an average transmit sensitivity of 0.4 kPa/V at 6 mm. From the PZFlex simulations, we estimated an output pressure of 50 kPa/V at the surface of one element, in agreement with [42]–[45].

B. Receive Characterization

Fig. 10(a) shows the SNR for all the 64 RX elements as computed from the PE measurements using the tungsten wire. The four values marked in red correspond to the elements having an SNR more than 6 dB below the mean value. Fig. 10(c) shows that these elements are located at the edges of the transducer aperture, which is the most critical area in

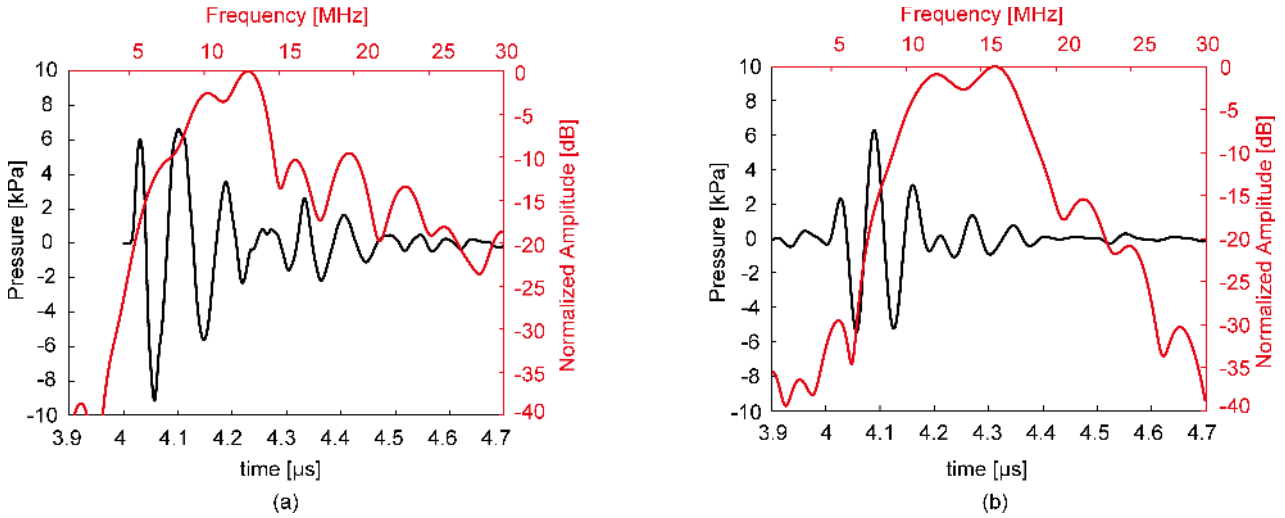

Fig. 8. Transmit pressure at a depth of 6 mm and the corresponding spectra from (a) FEM simulations and (b) measurements of one TX element.

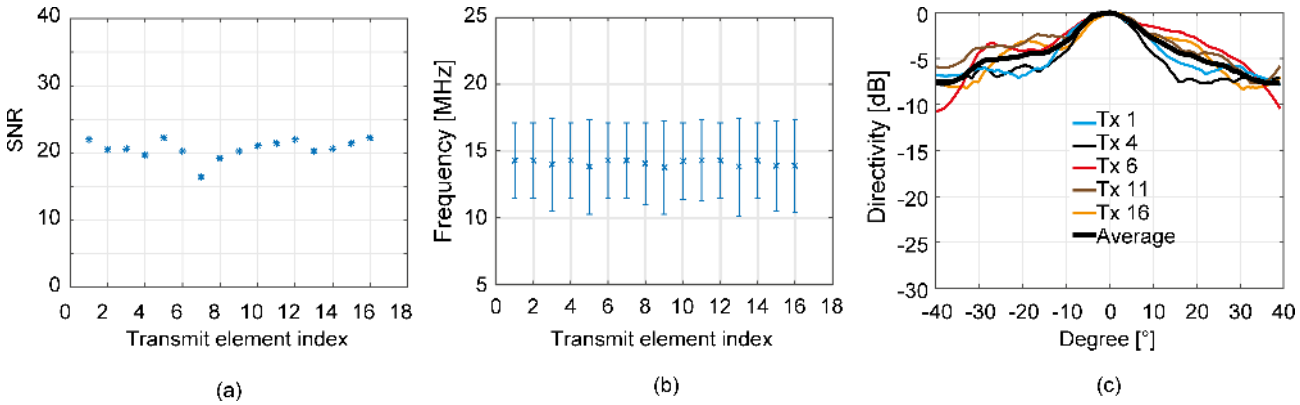

Fig. 9. Measured (a) SNR and (b) center frequency with −3-dB bandwidth across the 16 TX elements. (c) Directivity for five transmit elements and average directivity pattern.

TABLE V
TRANSMIT PERFORMANCE

	Measurement		Simulation
	mean	STD	
f_c [MHz]	14	0.2	13
BW_{-3dB} [%]	44	5.4	38
Pressure peak-to-peak @ 6 mm [kPa]	11	1.6	17

terms of mechanical stability. The poor performance of these elements can be attributed to the fabrication process, which requires removal of any epoxy residue from the area of the five bond pads. This process is presently difficult to control and can easily lead to damages of the elements on the edges.

Fig. 10(b) shows, for the remaining 60 RX elements, the center frequency, and −6-dB bandwidth. The average center frequency is 14 MHz, and the average −6-dB bandwidth is 42%, in agreement with the values obtained for the TX elements. RX elements with index 19 and 57, although having SNR values close to 20 dB, have quite narrow bandwidth (less than 20%), which could be caused by defects in the material layers, since also these elements are located at the edge [Fig. 10(c)].

PZFlex simulation results showed an element impedance of approximately 5 kΩ at resonance. For the AFE, the SPICE-type simulator showed an input impedance of approximately 2 kΩ at resonance. With these impedance values, more than 70% of the signal can be read-out by the AFE, which is acceptable since the attenuation can be compensated by the PGA in the AFE. The *RC* equivalent circuit that was fit to the simulated impedance of the AFE resulted in a resistance and capacitance value of 8.05 kΩ and 6.45 pF, respectively. These values were used in PZFlex for the receive sensitivity computation.

To compute the receive sensitivity, we first characterize the gain of the receive signal chain with the PGA set to 18 dB [Fig. 11(a)]. The average gain at the center frequency (14 MHz) is 111.6 dBΩ. The PE peak-to-peak voltage amplitude obtained from the steel plate for neighboring TX/RX elements is then corrected for the electronic transfer function in receive giving the peak-to-peak current values

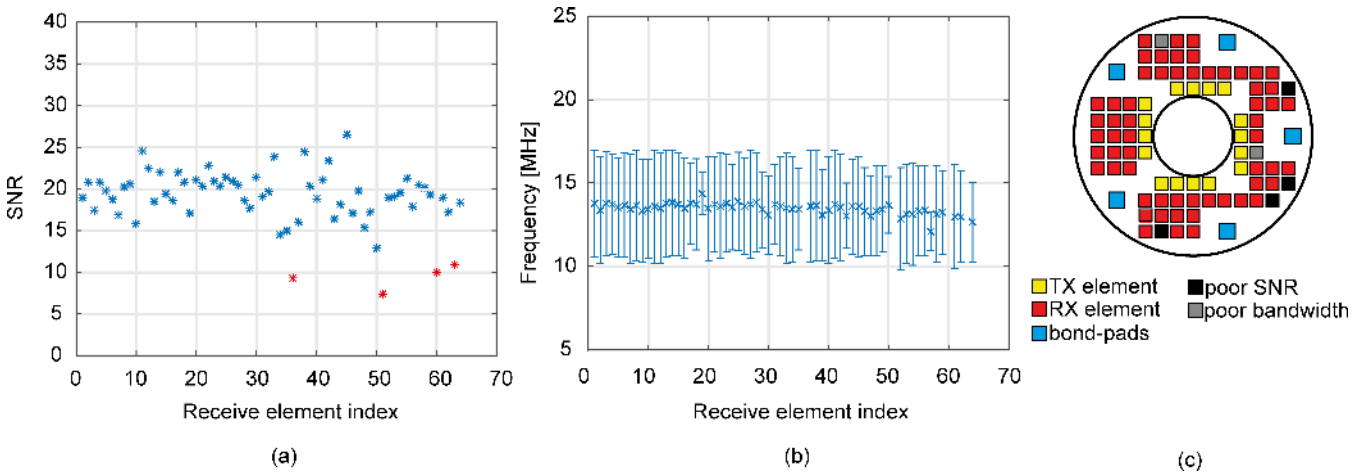

Fig. 10. Receive PE measurements with a tungsten wire. (a) SNR values for each receive element with defective elements marked in red. (b) Center frequency and −6-dB bandwidth across the receive elements (excluding the elements with low SNR). (c) Location of the defective elements in the transducer layout.

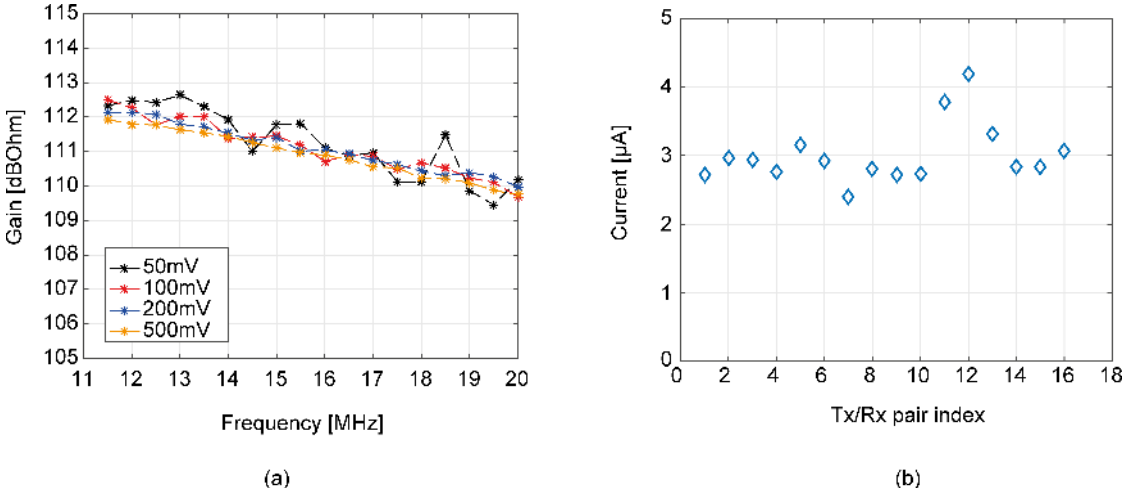

Fig. 11. (a) AFE gain of the receive chain over frequency for different amplitude settings with the PGA set to 18 dB. (b) Peak-to-peak current amplitude over the elements for PE measurements where each of the TX elements transmits individually and the closest RX element is considered in RX.

shown in Fig. 11(b), with an average value of 3 μA. The simulated current through the element for the same pressure load as in the measurements and with the element electrically loaded by the equivalent model of the front-end receiver input impedance is 2.9 μA. The simulated and measured current values are in a very good agreement. Therefore, we estimate the (electrically unloaded) receive sensitivity based on simulation results, since PZFlex allows modeling the element in unloaded condition and computing the voltage over the element for a certain input pressure. The receive sensitivity value thus found is 3.7 μV/Pa.

We also simulated and measured the input referred noise of the analog receive signal chain [Fig. 12(a)]. The measured integrated noise within the bandwidth of 10–16 MHz is around 2.53 nA, in good agreement with the simulated value of 2.3 nA. The transducer in-band rms noise is around 4.4 nA, hence dominating over the AFE, as desirable. The overall noise figure is approximately 1.2 dB. Considering the transducer element impedance at resonance (approximately 5 kΩ) and the element receive sensitivity, the expected minimum detectable pressure is approximately 10 Pa. Fig. 12(b) shows the dynamic range for the three gain settings of the PGA The minimum detectable signal can be obtained at the 0-dB cross-point in the lowest gain setting and the maximum signal that the circuit can handle can be obtained at the SNR saturation cross point in the highest gain setting. Therefore, the dynamic range is approximately 55 dB.

C. Imaging

Fig. 13(a) shows the maximum projections along y and x of the 3-D image of the three spheres obtained using DAS, whereas Fig. 13(b) shows the maximum projections for the image obtained using the CF method.

For the scatterer at 6.5 mm, the −6-dB lateral width is 560 μm using standard DAS, in agreement with the value obtained from the simulated field-II image [Fig. 4(d)]. By implementing the CF method, the −6-dB lateral width is reduced to 320 μm. Overall, the image obtained using the CF shows fewer artifacts and better resolution. The 3-D rendering of the three spherical targets is shown in Fig. 13(c).

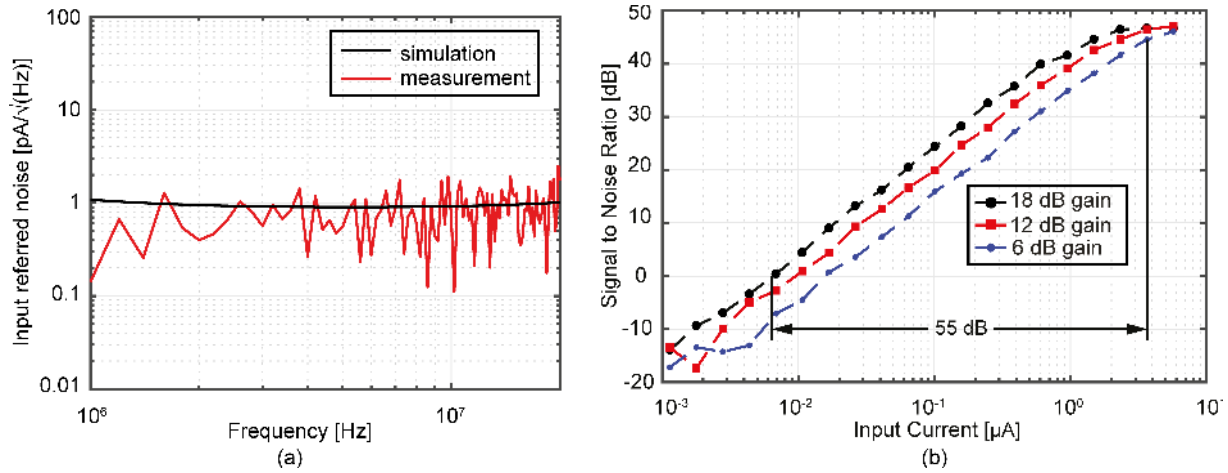

Fig. 12. (a) Simulated and measured input referred noise over frequency of the AFE and (b) dynamic range for different gain settings of the PGA.

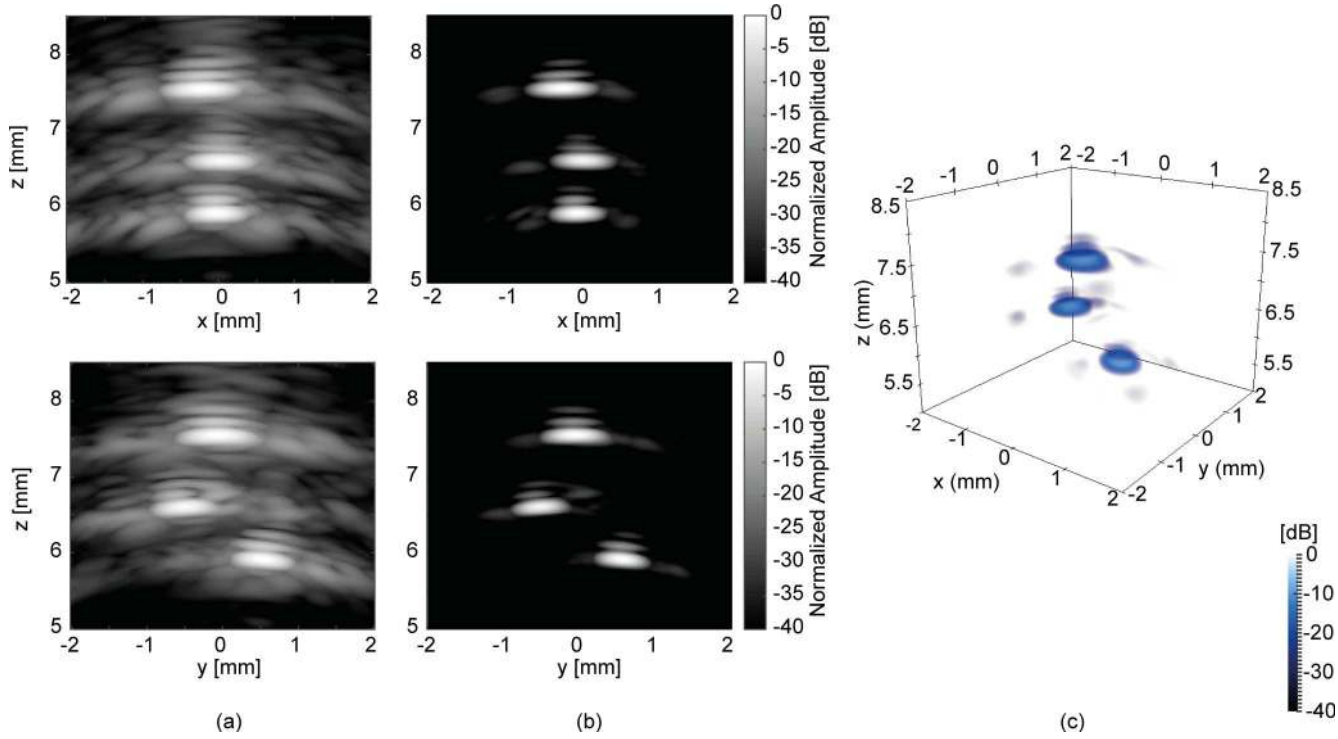

Fig. 13. Maximum projections along y and x from 3-D FL images using (a) DAS and (b) CF. (c) 3-D rendering of the three spheres obtained with the CF method.

V. Discussion and Conclusion

In this work, we have presented a 14-MHz 2-D matrix ultrasound transducer for FL-IVUS imaging that is integrated with a front-end ASIC requiring only four cables. We first investigated potential transducer designs using field II. The design with the transmit elements around the inner hole and the receivers on a regular grid pattern (design C) shows good performances with low sidelobe levels. Since this design can be manufactured using well-established dicing technology, we opted for it and further adjusted it to accommodate the five bond pads required to connect four cables (with the fifth pad connected to the ground shield). Compared to [30] and [31] our transmit aperture is smaller; hence, the PSF is degraded compared to a ring array. However, we used the d_{33} mode which is 2 times more sensitive than the d_{31} used in [30] and [31].

The switches and multiplexer on the ASIC allow transmitting with one or multiple TX elements, whereas the received signal can be acquired with one RX at the time. Considering that the maximum imaging depth required for FL-IVUS is ~10 mm [9], a full synthetic-aperture scheme can be achieved with volume frame rates on the order of 100 Hz, which is adequate for real-time imaging of CTOs.

We have successfully manufactured the complete transducer on top of the ASIC and characterized it acoustically both in transmit and in receive. Fairly good agreement is present between the simulated and measured results for the transmit and receive behavior. Despite inaccuracies in the simulations,

such as the material properties, the PZFlex model provided an acceptable estimate of the overall transducer behavior, allowing also estimating the element receive sensitivity in unloaded conditions.

We performed imaging measurements using spherical steel reflectors, showing the capability of the device to generate 3-D FL images. Artifacts behind the main signal of the sphere are visible in the images. The cause of these artifacts is the presence of the ASIC behind the transducer, which does not act as a standard backing and causes ringing. A proper dematching layer should be developed to reduce the ringing effect [46] similar to the approach in [32]. Moreover, some elements on the edges showed poor performance, resulting in low SNR and poor bandwidth. These elements are in general more prone to damage due to their peripheral location and proximity to the bondpads, which leads to mechanical instability.

The acoustic characterization and the initial imaging measurements showed promising results. In the future, parylene coating should be used to insulate the transducer. The thickness of this layer is of only 1–2 microns; therefore, we do not expect significant changes in the acoustic properties.

Future work will also include the development of 2-D matrix transducers using laser cutting technology. By laser cutting the individual transducer elements, nongridded 2-D matrix transducers with variable pitch can be achieved. This will lead to better imaging capability and reduced artifacts as shown in the simulation results for design ***D*** in Fig. 2.

In conclusion, the proposed 2-D matrix transducer with front-end ASIC and low cable count opens the doors for different possibilities that could lead to FL-IVUS catheters with steerable mechanisms for image guidance during CTO crossing procedures.

ACKNOWLEDGMENT

J. Janjic would like to thank Oldelft B.V., Delft, The Netherlands, for providing materials for the transducer acoustic stack.

REFERENCES

[1] *Cardiovascular Diseases (CVDs)*, World Health Org., Geneva, Switzerland, Jun. 2017.

[2] R. Ross, "Atherosclerosis—An inflammatory disease," *New England J. Med.*, vol. 340, pp. 115–126, Jan. 1999.

[3] R. Virmani, F. D. Kolodgie, A. P. Burke, A. Farb, and S. M. Schwartz, "Lessons from sudden coronary death: A comprehensive morphological classification scheme for atherosclerotic lesions," *Arterioscleros, Thrombosis, Vascular Biol.*, vol. 20, no. 5, pp. 1262–1275, 2000.

[4] H. M. Garcia-Garcia, M. A. Costa, and P. W. Serruys, "Imaging of coronary atherosclerosis: Intravascular ultrasound," *Eur. Heart J.*, vol. 31, pp. 2456–2469, Oct. 2010.

[5] H. M. Garcia-Garcia, B. D. Gogas, P. W. Serruys, and N. Bruining, "IVUS-based imaging modalities for tissue characterization: Similarities and differences," *Int. J. Cardiovascular Imag.*, vol. 27, pp. 215–224, Feb. 2011.

[6] C. L. de Korte, H. H. Hansen, and A. F. van der Steen, "Vascular ultrasound for atherosclerosis imaging," *Interface Focus*, vol. 1, pp. 565–575, Aug. 2011.

[7] M. O'Donnell, M. J. Eberle, D. N. Stephens, J. L. Litzza, K. S. Vicente, and B. M. Shapo, "Synthetic phased arrays for intraluminal imaging of coronary arteries," *IEEE Trans. Ultrason., Ferroelectr., Freq. Control*, vol. 44, no. 3, pp. 714–721, May 1997.

[8] W. C. Black, Jr. and D. N. Stephens, "CMOS chip for invasive ultrasound imaging," *IEEE J. Solid-State Circuits*, vol. 29, no. 11, pp. 1381–1387, Nov. 1994.

[9] B. K. Courtney *et al.*, "Innovations in imaging for chronic total occlusions: A glimpse into the future of angiography's blind-spot," *Eur. Heart J.*, vol. 29, pp. 583–593, Mar. 2008.

[10] G. W. Stone *et al.*, "Percutaneous recanalization of chronically occluded coronary arteries: A consensus document: Part I," *Circulation*, vol. 112, no. 15, pp. 2364–2372, 2005.

[11] J. L. Evans *et al.*, "Arterial imaging with a new forward-viewing intravascular ultrasound catheter, I. Initial studies," *Circulation*, vol. 89, pp. 712–717, Feb. 1994.

[12] K. H. Ng *et al.*, "Arterial imaging with a new forward-viewing intravascular ultrasound catheter, II. Three-dimensional reconstruction and display of data," *Circulation*, vol. 89, pp. 718–723, Feb. 1994.

[13] J. H. Rogers, "Forward-looking IVUS in chronic total occlusions," in *Cardiac Interventions Today*. Wayne, PA, USA: BMC, 2009.

[14] D. T. Raphael *et al.*, "20 MHz Forward-imaging single-element beam steering with an internal rotating variable-angle reflecting surface: Wire phantom and *ex vivo* pilot study," *Ultrasonics*, vol. 53, pp. 561–569, Feb. 2013.

[15] D. H. Liang and B. S. Hu, "Forward viewing ultrasonic imaging catheter," U.S. Patent 5 651 366, Jul. 29, 1997.

[16] D. N. Stephens *et al.*, "Experimental studies with a 9F forward-looking intracardiac imaging and ablation catheter," *J. Ultrasound Med.*, vol. 28, no. 2, pp. 207–215, Feb. 2009.

[17] A. Bezanson, R. Adamson, and J. A. Brown, "Fabrication and performance of a miniaturized 64-element high-frequency endoscopic phased array," *IEEE Trans. Ultrason., Ferroelectr., Freq. Control*, vol. 61, no. 1, pp. 33–43, Jan. 2014.

[18] R. Chen *et al.*, "PMN-PT single-crystal high-frequency kerfless phased array," *IEEE Trans. Ultrason., Ferroelectr., Freq. Control*, vol. 61, no. 6, pp. 1033–1041, Jun. 2014.

[19] E. D. Light and S. W. Smith, "Two dimensional arrays for real time 3D intravascular ultrasound," *Ultrason. Imag.*, vol. 26, pp. 115–128, Apr. 2004.

[20] E. D. Light, J. F. Angle, and S. W. Smith, "Real-time 3-D ultrasound guidance of interventional devices," *IEEE Trans. Ultrason., Ferroelectr., Freq. Control*, vol. 55, no. 9, pp. 2066–2078, Sep. 2008.

[21] F. L. Degertekin, R. O. Guldiken, and M. Karaman, "Annular-ring CMUT arrays for forward-looking IVUS: Transducer characterization and imaging," *IEEE Trans. Ultrason., Ferroelectr., Freq. Control*, vol. 53, no. 2, pp. 474–482, Feb. 2006.

[22] B. T. Khuri-Yakub and Ö. Oralkan, "Capacitive micromachined ultrasonic transducers for medical imaging and therapy," *J. Micromech. Microeng.*, vol. 21, p. 054004, May 2011.

[23] C. Tekes *et al.*, "3-D real-time volumetric imaging using 20 MHz 1.5-mm diameter single-chip CMUT-on-CMOS array," in *Proc. IEEE Int. Ultrason. Symp. (IUS)*, 2012, pp. 1–4.

[24] D. N. Stephens *et al.*, "First *in vivo* use of a capacitive micromachined ultrasound transducer array-based imaging and ablation catheter," *J. Ultrasound Med.*, vol. 31, no. 2, pp. 247–256, 2012.

[25] G. Gurun *et al.*, "Single-chip CMUT-on-CMOS front-end system for real-time volumetric IVUS and ICE imaging," *IEEE Trans. Ultrason., Ferroelectr., Freq. Control*, vol. 61, no. 2, pp. 239–250, Feb. 2014.

[26] C. Tekes *et al.*, "Real-time imaging system using a 12-MHz forward-looking catheter with single chip CMUT-on-CMOS array," in *Proc. IEEE Int. Ultrason. Symp. (IUS)*, Oct. 2015, pp. 1–4.

[27] M. Pekař *et al.*, "Preclinical testing of frequency-tunable capacitive micromachined ultrasonic transducer probe prototypes," *Ultrasound Med. Biol.*, vol. 43, no. 9, pp. 2079–2085, 2017.

[28] Ö. Oralkan *et al.*, "Capacitive micromachined ultrasonic transducers: Next-generation arrays for acoustic imaging?" *IEEE Trans. Ultrason., Ferroelectr., Freq. Control*, vol. 49, no. 11, pp. 1596–1610, Nov. 2002.

[29] A. S. Ergun, G. G. Yaralioglu, and B. T. Khuri-Yakub, "Capacitive micromachined ultrasonic transducers: Theory and technology," *J. Aerosp. Eng.*, vol. 16, no. 2, pp. 76–84, Apr. 2003.

[30] Y. Wang, D. N. Stephens, and M. O'Donnell, "Optimizing the beam pattern of a forward-viewing ring-annular ultrasound array for intravascular imaging," *IEEE Trans. Ultrason., Ferroelectr., Freq. Control*, vol. 49, no. 12, pp. 1652–1664, Dec. 2002.

[31] Y. Wang, D. N. Stephens, and M. O'Donnell, "Initial results from a forward-viewing ring-annular ultrasound array for intravascular imaging," in *Proc. IEEE Ultrason. Symp.*, vols. 1–2, Oct. 2003, pp. 212–215.

[32] D. Wildes *et al.*, "4-D ICE: A 2-D array transducer with integrated ASIC in a 10-Fr catheter for real-time 3-D intracardiac echocardiography," *IEEE Trans. Ultrason., Ferroelectr., Freq. Control*, vol. 63, no. 12, pp. 2159–2173, Dec. 2016.

[33] J. Janjic *et al.*, "Sparse ultrasound image reconstruction from a shape-sensing single-element forward-looking catheter," *IEEE Trans. Biomed. Eng.*, to be published.
[34] M. Tan *et al.*, "A front-end ASIC with high-voltage transmit switching and receive digitization for forward-looking intravascular ultrasound," in *Proc. IEEE Custom Integr. Circuits Conf. (CICC)*, Apr./May 2017, pp. 1–4.
[35] J. A. Jensen, "Field: A program for simulating ultrasound systems," *Med. Biol. Eng. Comput.*, vol. 4, no. 1, pp. 351–353, 1996.
[36] J. A. Jensen and S. I. Nikolov, "Fast simulation of ultrasound images," in *Proc. IEEE Ultrason. Symp.*, vols. 1–2, Oct. 2000, pp. 1721–1724.
[37] J. A. Jensen and N. B. Svendsen, "Calculation of pressure fields from arbitrarily shaped, apodized, and excited ultrasound transducers," *IEEE Trans. Ultrason., Ferroelectr., Freq. Control*, vol. 39, no. 2, pp. 262–267, Mar. 1992.
[38] A. Ramalli, E. Boni, A. S. Savoia, and P. Tortoli, "Density-tapered spiral arrays for ultrasound 3-D imaging," *IEEE Trans. Ultrason., Ferroelectr., Freq. Control*, vol. 62, no. 8, pp. 1580–1588, Aug. 2015.
[39] N. N. Abboud, G. L. Wojcik, D. K. Vaughan, J. Mould, D. J. Powell, and L. Nikodym, "Finite element modeling for ultrasonic transducers," *Ultrason. Transducer Eng.*, vol. 3341, pp. 19–42, May 1998.
[40] C. Chen *et al.*, "A prototype PZT matrix transducer with low-power integrated receive ASIC for 3-D transesophageal echocardiography," *IEEE Trans. Ultrason., Ferroelectr., Freq. Control*, vol. 63, no. 1, pp. 47–59, Jan. 2016.
[41] K. W. Hollman, K. W. Rigby, and M. O'Donnell, "Coherence factor of speckle from a multi-row probe," in *Proc. IEEE Ultrason. Symp.*, vols. 1–2, Oct. 1999, pp. 1257–1260.
[42] J. G. Knight and F. L. Degertekin, "Fabrication and characterization of cMUTs for forward looking intravascular ultrasound imaging," in *Proc. IEEE Ultrason. Symp.*, vols. 1–2, Oct. 2003, pp. 1175–1178.
[43] O. Oralkan, S. T. Hansen, B. Bayram, G. G. Yaralioglu, A. S. Ergun, and B. T. Khuri-Yakub, "CMUT ring arrays for forward-looking intravascular imaging," in *Proc. IEEE Ultrason. Symp.*, vol. 1, Aug. 2004, pp. 403–406.
[44] F. L. Degertekin, R. O. Guldiken, and M. Karaman, "Micromachined capacitive transducer arrays for intravascular ultrasound," *MOEMS Display Imag. Syst. III*, vol. 5721, pp. 104–114, Jan. 2005.
[45] A. Nikoozadeh *et al.*, "Forward-looking intracardiac ultrasound imaging using a 1-D CMUT array integrated with custom front-end electronics," *IEEE Trans. Ultrason., Ferroelectr., Freq. Control*, vol. 55, no. 12, pp. 2651–2660, Dec. 2008.
[46] J.-F. Gelly, D. M. Mills, F. Lanteri, C. E. Baumgartner, and S. G. Calisti, "Method for optimized dematching layer assembly in an ultrasound transducer," U.S. Patent 7 621 028, Nov. 24, 2009.

Jovana Janjic received the B.Sc. degree in information engineering and the M.Sc. degree in bioengineering from The University of Padua, Padua, Italy, in 2011 and 2013, respectively, and the Ph.D. degree in biomedical engineering from Erasmus Medical Center, Rotterdam, The Netherlands, in 2018. At the Royal Institute of Technology (KTH), Stockholm, Sweden, she completed her master's thesis on sonothrombolysis using contrast agents.

She was selected within the Erasmus Program as an Exchange Student at KTH from 2012 to 2013. Her research interests include intravascular ultrasound imaging, transducer design, and evaluation.

Mingliang Tan received the B.S. degree in electronic science and technology from Northeastern University, Shenyang, China, in 2014, and the M.S. degree in microelectronics from the Delft University of Technology, Delft, The Netherlands, in 2016, where he is currently pursuing the Ph.D. degree in electrical engineering with the Electronic Instrumentation Laboratory, with a focus on ASIC design for medical ultrasound imaging.

His research interests include analog and mixed-signal electronics, especially for biomedical applications.

Verya Daeichin was born in Kermanshah, Iran, in 1984. He received the bachelor's degree in bioelectric engineering from the Biomedical Engineering Department, Amirkabir University of Technology (Tehran Polytechnic), Tehran, Iran, in 2008, the first master's degree in biomedical signal processing and pattern recognition from the University of Boras, Boras, Sweden, and the second master's degree in biomedical image processing from the Chalmers University of Technology, Gothenburg, Sweden. Since 2010, he has been pursuing the Ph.D. degree with Erasmus Medical Center, Rotterdam, The Netherlands.

His research area is molecular imaging using target microbubble contrast agents.

Emile Noothout graduated from Intermediate Technical School for Mechanics, Dordrecht, The Netherlands, in 2004. Then, he studied for Research Instrument Maker at Leidse Instrumentmaker School, Leiden, The Netherlands, from 2004 to 2006.

From 2007 to 2013, he worked as a Research Instrument Maker with TNO, Delft, The Netherlands. Since 2013, he worked as been with the Delft University of Technology, Delft, where he is involved in the development of medical ultrasound transducers and research assistance.

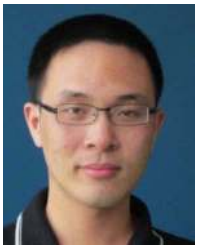

Chao Chen received the B.Sc. degree in microelectronics from Tsinghua University, Beijing, China, in 2010, the M.Sc. degree (*cum laude*) in microelectronics from the Delft University of Technology, Delft, The Netherlands, in 2012, and the Ph.D. degree in electrical engineering from the Electronic Instrumentation Laboratory, Delft University of Technology, with a focus on ASIC design for medical ultrasound imaging.

His research interests include integrated circuits for medical ultrasound imaging and data converters. Dr. Chen was a recipient of the Huygens Scholarship in 2011.

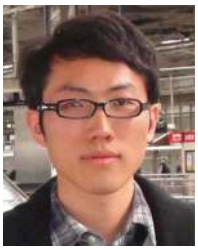

Zhao Chen received the B.S. degree in microelectronics from Fudan University, Shanghai, China, in 2011, and the M.S. degree in electrical and electronic engineering from Imperial College, London, U.K., in 2012. He is currently pursuing the Ph.D. degree in electrical engineering with the Delft University of Technology, Delft, The Netherlands., with a focus on the ASIC design for 3-D medical ultrasound imaging.

His research interests include analog and mixed-signal electronics, especially for biomedical application.

Zu-Yao Chang received the M.Sc. degree in electrical engineering from the Delft University of Technology, Delft, The Netherlands, in 2003.

Since 2003, he has been a Staff Member with the Electronic Instrumentation Laboratory, Delft University of Technology, focusing on impedance measurement systems and smart sensor systems.

Robert H. S. H. Beurskens received the B.Sc. degree in electrical engineering from the Fontys Hogeschool Venlo, Venlo, The Netherlands.

He was an electrical engineer with Hauzer Techno Coating, Venlo, focusing on industrial scale physical vapor deposition equipment. In 1999, he joined the Prins Maurits Laboratorium, Rijswijk, The Netherlands, a branch of the Dutch organization for applied physics TNO. His main interest was the design, construction, and operation of high-voltage pulsed-power systems for all kinds of civil and defense applications varying from foodstuff sterilization, atmospheric plasma's to electric reactive armor, and counter measures. Since 2007, he has been an Electronic Designer and an Instrumentation Technician with the Department of Biomedical Engineering, Erasmus Medical Center, Rotterdam, The Netherlands. The main interests here are analog and high-frequency electronics for ultrasound applications.

Gijs van Soest received the M.Sc. degree in physics from the University of Groningen, Groningen, The Netherlands, in 1997, and the Ph.D. degree from the University of Amsterdam, Amsterdam, The Netherlands, in 2001, with a focus on the interplay of light scattering and laser physics.

From 2002 to 2005, he was with the Royal Netherlands Meteorology Institute, De Bilt, The Netherlands, and the Space Research Organization of the Netherlands, Groningen, The Netherlands, where he focused on remote sensing of atmospheric trace gases and satellite validation. In 2005, he held a post-doctoral position at the Thoraxcenter, Rotterdam, The Netherlands, for a project on OCT elastography. Since then, his activities have broadened to include catheter development, automatic image analysis, and high-frequency ultrasonic imaging. In 2010, he was appointed Assistant Professor and became a Staff Member of the Department of Biomedical Engineering. His research focuses on the use and development of intravascular imaging methods for detection of coronary atherosclerosis, on optical coherence tomography, specifically on methods for functional imaging, and on intravascular photoacoustic imaging. These developments are carried out in close collaboration with clinicians of the Department of Interventional Cardiology.

Antonius F. W. van der Steen (M'94–SM'03–F'13) received the M.Sc. degree in applied physics from Technical University Delft, Delft, The Netherlands, in 1989, and the Ph.D. degree in medical sciences from the University of Nijmegen, Nijmegen, The Netherlands, in 1994.

From 1994 to 1996, he was a Senior Scientist with the Laboratory for Experimental Echocardiography, Thoraxcenter, Rotterdam, The Netherlands, and since 1997, he has been the Head of this laboratory. Since 2002, he has been a Full Professor and the Head of biomedical engineering at Erasmus MC, Rotterdam. Since 2013, he has been a Full Professor of applied physics with the Technical University Delft, and an honorary Visiting Professor with the Chinese Academy of Sciences, Shenzhen Institutes of Advanced Technologies, Shenzhen, The Netherlands. His current research interests are in vulnerable plaque detection, intravascular imaging, biomechanics, ultrasound contrast agents, and transducer design for special applications.

Dr. van der Steen is a member of the Royal Dutch Academy of Science (KNAW) and the Netherlands Academy of Technology and Innovation (i.e., the Dutch Academy of Engineering). He is a fellow of the European Society of Cardiology. He is the 2000 NWO PIONIER Technical Sciences (best researcher of the Netherlands in technical science under 40), and the 2007 Simon Stevin Master (best researcher in translational research).

Martin D. Verweij (M'10) received the M.Sc. degree (*cum laude*) in electrical engineering and the Ph.D. degree in electrical engineering from the Delft University of Technology, Delft, The Netherlands, in 1988 and 1992, respectively.

From 1993 to 1997, he was a Research Fellow with the Royal Netherlands Academy of Arts and Sciences, Amsterdam, The Netherlands. In 1998, he became an Associate Professor with the Laboratory of Electromagnetic Research, Delft University of Technology, where he joined the Laboratory of Acoustical Wavefield Imaging in 2011. His research interests include dedicated transducer design, beamforming algorithms, and the theoretical modeling and numerical simulation of medical ultrasound.

Dr. Verweij is an Associate Editor of the *Journal of the Acoustical Society of America*.

Michiel A. P. Pertijs (S'99–M'06–SM'10) received the M.Sc. and Ph.D. degrees (*cum laude*) in electrical engineering from Delft University of Technology, Delft, The Netherlands, in 2000 and 2005, respectively.

From 2005 to 2008, he was with National Semiconductor, Delft, where he designed precision operational amplifiers and instrumentation amplifiers. From 2008 to 2009, he was a Senior Researcher with imec/Holst Centre, Eindhoven, The Netherlands. In 2009, he joined the Electronic Instrumentation Laboratory, Delft University of Technology, where he is currently an Associate Professor. He heads a research group, focusing on integrated circuits for medical ultrasound and energy-efficient smart sensors. He has authored or coauthored two books, three book chapters, 12 patents, and over 80 technical papers.

Dr. Pertijs received the ISSCC 2005 Jack Kilby Award for Outstanding Student Paper and the JSSC 2005 Best Paper Award. For his Ph.D. research on high-accuracy CMOS smart temperature sensors, he received the 2006 Simon Stevin Gezel Award from the Dutch Technology Foundation STW. In 2014, he was elected Best Teacher of the EE program at Delft University of Technology. He serves as an Associate Editor for the IEEE JOURNAL OF SOLID-STATE CIRCUITS. He also served on the program committees of International Solid-State Circuits Conference (ISSCC), the European Solid-State Circuits Conference (ESSCIRC), and the IEEE Sensors Conference.

Nico de Jong (A'97–M'09) received the M.Sc. degree in physics from Delft University of Technology, Delft, The Netherlands, in 1978, and the Ph.D. degree in acoustic properties of ultrasound contrast agents from the Erasmus Medical Center, Rotterdam, The Netherlands, in 1993.

Since 1980, he has been a Staff Member with the Thoraxcenter, Erasmus Medical Center. In 2003, he became a part-time Professor with the University of Twente, Enschede, The Netherlands. Over the last five years, he has given more than 30 invited lectures and has given numerous scientific presentations for international industries. He teaches on Technical Universities and the Erasmus MC. He has been the promotor of 21 Ph.D. students and is currently supervising 11 Ph.D. students. Since 2011, he has been a Professor of molecular ultrasonic imaging and therapy with the Erasmus MC and the Technical University of Delft, Delft.

Dr. de Jong is an Organizer of the annual European Symposium on Ultrasound Contrast Imaging, held in Rotterdam and attended by approximately 175 scientists from universities and industries all over the world. He is on the safety committee of World Federation of Ultrasound in Medicine and Biology (WFUMB), an Associate Editor of UMB, and has been a Guest Editor for special issues of different journals.